

Design and Prototyping of a Transformable Quadruped Robot

An Undergraduate Honors Thesis

Presented to The Department of Mechanical Engineering

The Ohio State University

In Partial Fulfillment of the Requirements for  
Graduation with Distinction in Mechanical Engineering

by

Yupeng Cheng

April 2018

Advisor: Haijun Su, Ph.D.

## Abstract

Quadruped robotic mechanism is a legged robotic structure using four legs to move. In many legged robotic structures, quadruped is the ideal one for mobility performance and efficiency. Quadruped robots features more stable and more smooth movement than wheeled robots on rough and complex terrains. Wheeled robots featuring moving on wheels is another structure different than legged robotic structure. It can move faster on flat and less rough terrains than the quadrupeds. For quadruped and wheeled structures, either one can fail to move properly once the terrains are inappropriate. Correspondingly, to have a robotic structure performing well under whatever terrain conditions is highly demanded. To solve the demand, the transformation mechanism is a solution. This research designs and prototypes a transformable quadruped robot with its transformation mechanism, so it can transform between the quadruped type and the wheeled type freely depending on the terrain conditions. The research requires the knowledge and the techniques on dynamics, kinematics, materials, and machining. Due to the time limit, the project ends up at the 1st complete prototype of one identical leg with a transformation mechanism. Actuator test is complete, and more tests and future work are in plan.

## Acknowledgement

I would like to thank Dr. Haijun Su for the opportunity to be his undergraduate research assistant and to contribute my knowledge and techniques to the study of robotics. Dr. Su has supported this project in the Design Innovation and Simulation Laboratory (DISL). Equipment's and materials from the DISL are parts of keys that the project can achieve its desired goals.

I would like to thank Dr. Wei Zhang from ECE department for helping with his expertise on testing and hardware control.

I would like to thank PhD. Xianpai Zeng and Yu She for help on 3D printing and laser cutting.

I also would like to thank my partner, Guillermo Andrés Castillo Martínez, for helping on the testing setup, processes, and data collection and analysis.

Eventually, thank all who ever offered help physically and mentally. This project would be an impossible mission without your great help.

## Table of Contents

Abstract.....	ii
Acknowledgement .....	iii
List of Figures .....	vi
List of Tables .....	vii
Chapter 1: Introduction of the thesis.....	1
1.1 Legged Robots.....	1
1.2 Quadruped Robots.....	1
1.3 Wheeled Robots .....	4
1.4 Transformation mechanism.....	4
1.5 Objectives of this research .....	5
1.6 Overview of the thesis .....	5
Chapter 2: Design Specifications .....	6
2.1 Constraints .....	6
Chapter 3: Conceptual Design .....	7
3.1 Dimensioned design of the robot .....	7
3.2 Kinematics analysis .....	8
3.3 Approaches of the concepts of the transformation mechanism / actuators selection .....	12
3.4 D printing study .....	15
Chapter 4: Design of the transformable quadruped robot .....	17
4.1 Design of the forearm .....	17
4.2 Design of the main arm.....	18
4.3 Design of the shoulder .....	20
4.4 Design of the transformation process.....	21
4.5 Simulation of designed parts and assemblies.....	22
4.6 Trajectory generation .....	25
Chapter 5: Testing procedures and results .....	29
5.1 Goal of testing.....	29
5.2 Testing setup .....	29
5.3 The testing procedure.....	32

5.4 Testing results .....	32
5.5 Discussion of the leg motion testing .....	35
Chapter 6: Conclusions of the thesis.....	37
6.1 Contributions.....	37
6.2 Future work.....	38
6.2.1 Mechanical design: .....	38
6.2.2 Testing: .....	39
6.3 Summary of the thesis.....	39
Reference .....	41

## List of Figures

Figure 1 A: a mainframe; B: five-bar link systems; C: compliant feet; D: a direct-current motor; [2] .....	2
Figure 2 "Pitch", "Roll", and "Yaw" [4] .....	3
Figure 3 Stability margin value according to different locations of COM. COM: center of mass [6] .....	4
Figure 4 The conceptual design of the robot.....	8
Figure 5 Tiptoe trajectory of Cheetaroid II [2] .....	9
Figure 6 Angular acceleration at forearm joint .....	9
Figure 7 Angular acceleration at main arm joint .....	9
Figure 8 Angular velocity at forearm joint .....	10
Figure 9 Angular velocity at main arm joint.....	10
Figure 10 Working logic of two-actuator-package .....	13
Figure 11 A: legged structure mode; B: wheeled structure mode.....	14
Figure 12 Complete assembly of the leg.....	17
Figure 13 Prototype of the forearm.....	18
Figure 14 Exploded view of main arm assembly .....	19
Figure 15 Left: former forearm servo assembly; right: weak seat causes reaction torque.....	19
Figure 16 Shoulder assembly .....	20
Figure 17 Left: old design without isolation; right: current design with isolation.....	21
Figure 18 Transformation process .....	22
Figure 19 The schematics of the forearm's cross-section [14].....	24
Figure 20 Coordinate system setup.....	25
Figure 21 Inverse kinematics for leg position.....	27
Figure 22 Sets of $\theta_1$ and $\theta_2$ generated by the function .....	27
Figure 23 Angular displacement $\theta_1$ vs. time.....	28
Figure 24 Angular displacement $\theta_2$ vs. time .....	28
Figure 25 A: clamp; B: caliper for calibration; C: control board; D: Arduino; E: power; F: computer .....	30
Figure 26 Angular displacement of the forearm servo.....	30
Figure 27 Angular displacement of the main arm servo .....	31
Figure 28 Operating screen of Tracker .....	31
Figure 29 Comparison between actual motion loop and the designed trajectory at step 1 .....	33
Figure 30 Comparison between actual motion loop and the designed trajectory at step 3 .....	34
Figure 31 Comparison between time consumed for one cycle in 20 Hz and 40 Hz .....	35
Figure 32 FEA analysis of locked-joint(L) and tensegrity leg® under 1000 N vertical load.....	38

## List of Tables

Table 1 comparison of the torque load on the joint .....	11
Table 2 parameters of actuators of two-actuator-package .....	13
Table 3 parameters of micro electromagnetic tooth clutches .....	15
Table 4 parts' and assemblies' stress simulation .....	23
Table 5 coefficients of calculated polynomials with 95% confidence .....	35

## Chapter 1: Introduction of the thesis

### 1.1 Legged Robots

The legged structure is one of the robotic structures. The robot uses this structure to achieve the mobility via moving legs. It is a critical frontier at robotic research area at mechanical engineering discipline. Compared with other structures like flying robots, wheeled robots and track robots, the legged robotic structure requests higher demands on mechanical design, kinematics design, dynamics study, mechatronics and control at mechanical discipline. Because of the agility of legs, the legged robots can move on almost all kinds of terrains or mixed. For decades, the breakthroughs on legged robotic research have been widely applied to the industry: robotic arm, hydraulic actuation system, and prosthetics.

The main limitations for legged robots are the quality actuators and mechanical designs. The actuators that are widely used on legged robots is motors. Since the robot movement has the features of heavy torque, fast speed and frequent spin-direction switch, the bar for the qualified motors therefore rises. Therefore, research groups in this field prefer to choose expensive customized motors to fit the requirements. However, the expense on motors is unnecessary if the mechanical design is outstanding. In this research, motors are purchased off the shelf, and the focus is on the mechanical design. A design that offers a light, proper, and durable structure can reduce the load on the motors and save more materials, which expands the number of qualified motors.

### 1.2 Quadruped Robots

A quadruped robot uses four legs to achieve its mobility. Different quadruped robots have different mobility. The method to sort the differences is to calculate the degree of freedom (DOF) via concluding the linkages and the number of actuators. The core concept of this is the



constraint criterion for spatial mechanisms stated as Kutzbach-Grubler criterion, which depends on the type of pair and its constraint as stated in ref. [1]:

$$F = b (n - 1) - \sum p_i c_i$$

$F$  is the degree of freedom (DOF),  $b$  is the DOF capacity of the space,  $n$  is the number of links,  $p_i$  is the number of pairs of type  $i$ , and  $c_i$  is the degree of constraint (degree of freedom lost) at a pair of type  $i$ . The formula from ref. [1] evolves when the mechanism only has revolute joints:

$$F = b (n - j - 1) + j$$

$j$  here is the number of joints. Other elements represent the same as the core concept.

For quadruped robots, three levels of the DOF classifies the mobility. What listed here are the cases of different capability levels followed by the representative examples.

A lowest mobility capability quadruped robot with one-DOF means the robot has only one driving actuator and can only move forward and backward. In 2016, Byeonghun Na and Kyoungchul Kong built a one DOF quadruped robot prototype together [2]. This robot has no control or sensors, it is designed for quadruped robotic motion study inspired by quadruped animals. The four caterpillar bands at the center of its longitudinal leg base length wraps the only motor. The root of each leg linkage holds the other end of each band. The leg can only move forward and backward tracing one trajectory as engineered by the leg linkage.

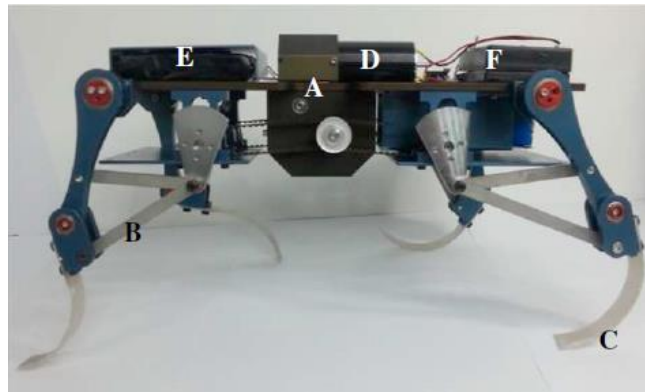


Figure 1 A: a mainframe; B: five-bar link systems; C: compliant feet; D: a direct-current motor; [2]

The second level of mobility capability is the DOF of the robot is a four. One representative example is the Cheetah-hub designed by BIOROB in 2013 [3]. Each leg of the robot has one driving motor. It hence is called the four-leg-drive robot. Each of its actuator sits at the frame link of the leg linkage. The leg linkage design dominates the leg motion trajectory. With the control board, the robot can finish the motions of pitch and yaw. However, limited by the number of actuators, the robot does not have DOF on “roll”. Figure 2 below shows the direction of "pitch", "yaw", and "roll" referring to the coordinate system.

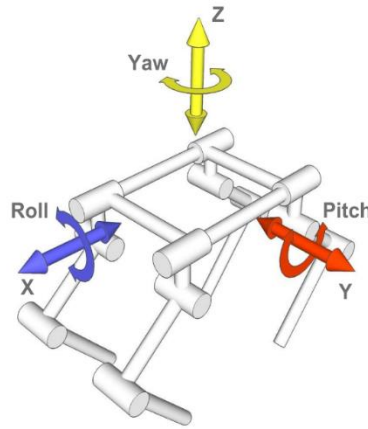


Figure 2 "Pitch", "Roll", and "Yaw" [4]

The top level of mobility capability is the 12-DOF quadruped robot. The most well-known product is Mini Spot made by Boston Dynamics [5]. This type has three actuators on each leg. Three actuators collaborate to complete the leg motion. Accordingly, the mobility of the robot includes the freedom on "pitch", "yaw", and "roll", the mobility in hence is better than the other two. Unlike the previous two types, the controller dominates the gait cycle of each leg. Therefore, the robot can have several trajectories.

In this research, the robot needs to have a DOF of 12 to study robotic control and trajectory generation as priorities. Given this, the main concentration of the mechanical design is on the structure design surviving from dynamic and static load.

### 1.3 Wheeled Robots

Wheeled robotics is a structure that differs from the legged structures. A robot with this structure moves via the spinning wheels. Yet, its mobility on stability cannot be as outstanding as a legged structured robot because the simple structure limits the scale of the motions on directions of "pitch", "yaw", and "roll" which are essential to obstacle avoidance. Wheeled robots obey the rules of vehicle dynamics. The geometries of "wheel bases on axis's", "steer ratio", and "roll angle" all impact the wheeled robots' mobility. Since the passive suspension system, a wheeled robot also has a narrow range of road grade due to its fixed center of mass (COM).

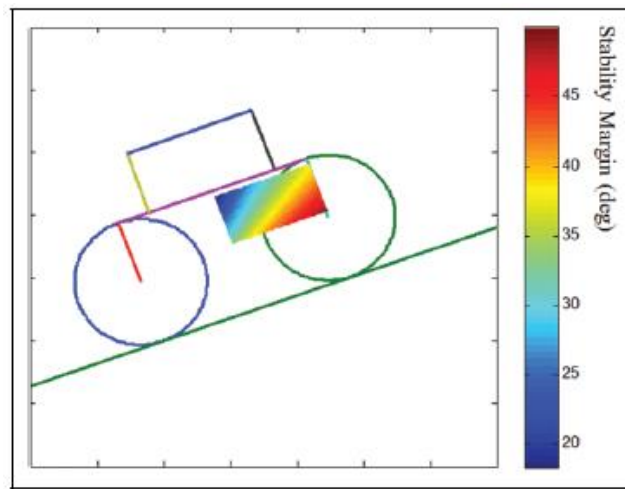


Figure 3 Stability margin value according to different locations of COM. COM: center of mass [6]

Besides the defects mentioned above, the wheeled structured robots feature moving fast on flat and low road-grade surfaces. This type also features more durable structure since the simplicity. A legged robot can never have the moving speed of a wheeled robot because of the linkage complexity and the non-linear trajectory velocities corresponding to the actuators.

### 1.4 Transformation mechanism

For the robot transformation in one structure type, wheeled robotics is a popular type because it has larger space of modification due to its simplicity of structure. In 2016, Inho Kim, Wonseok Jeon and Hyunseok Yang built a transforming wheeled robot to enhance mobility [6]. The robot transforms via shrinking/extending the wheelbases and adjusting flexible main body.

Considering the amount of work in the transformation is little, the transformation mechanism in this research is designed to be a solid structure rather than package of linkage. Doing so is to study the validity of having wheeled and legged structures on one robot. Therefore, design and prototype a solid transformation mechanism is a reasonable start of the research. Because of the two structures--wheeled and legged, the work load on each leg is greater than having one system. Given this, the transformation mechanism has higher demands on light weight and durability.

### 1.5 Objectives of this research

This research is to design and prototype a transformable quadruped robot with its transformation mechanism, so it can transform between the quadruped type and the wheeled type freely depending on the terrain conditions. Due to the limit of time, the research concentrates on design and prototyping one identical leg with its transformation mechanism. The focus is for the study of trajectory generation and actuator validity on the legged structure, so the theory of the wheeled structure and the transformation mechanism are included in the future work plan.

### 1.6 Overview of the thesis

This thesis comprises three chapters. Chapter 1 introduces the characters of legged robots, quadruped robots subordinate to legged robots and wheeled robots. Chapter 1 also introduces transformation mechanism and objectives of this research. Chapter 2 discusses the

constraints of the design. Chapter 3 discusses the conceptual design based on constraints, kinematics study, transformation solution, and actuator selection. Chapter 4 discusses the detailed design of each main part with its corresponding simulations. Chapter 5 is about the testing purpose, setup, results and conclusion. Chapter 6 is the thesis conclusion and the future work.

## Chapter 2: Design Specifications

### 2.1 Constraints

- The robot can switch freely between quadruped legged structure and wheeled structure when there is a need. Either structure can move fine.
- The robot is capable of all three motions of "pitch", "yaw" and "roll".
- Volumetric limit of 550mm x 550mm x 550mm.

Since the main material of most customized parts is PLA plastic, the volume of the robot should not to be larger than the number above to ensure the strength and that the robot does not crash by its own weight. Most PLA parts are made via 3D printers, the working space of the 3D printer also limits the volume of the robot.

- Commercial actuators

The team starts with commercial actuators rather than customized actuators. Customized actuators are usually considered when there is a complete prototype and completed tests. After

the actuator performances are defined from the tests, then there is a good opportunity for actuator customization.

- Mass of the whole robot should be less than 6kg.

Mass of each leg with its actuators limits at 1kg and the one of the main body with the rest of electronics limits at 2kg.

- Work load of the robot is greater than 1kg.
- Assembly issue free.

### Chapter 3: Conceptual Design

Based on the constraints given in the previous chapter, the next stage is to do concept design, kinematics study, transformation solution, and actuator selection which are the main contents of this chapter.

#### 3.1 Dimensioned design of the robot

The dimension sketch design is inspired by the 1-DOF quadruped robot -- Cheetaroid II - built by Byeonghun Na and Kyoungchul Kong [2]. The robot they built simulates the leg motions of animals. Therefore, Cheetaroid theoretically has a close trajectory to the animal leg motions under the geometry of its legs and the main body. Additionally, a model close to its geometry shall be capable of simulating similar leg motion. Hence the sketch dimension has scalar similarity to Cheetaroid II.

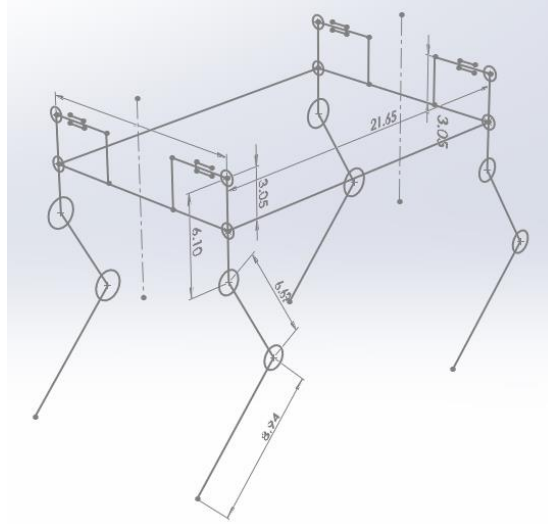


Figure 4 The conceptual design of the robot

Within the volumetric constraint, the length of the forearm of the identical leg is 227mm; the length of the main arm is 170mm; and the length and the width of the main body is 350mm and 550mm respectively. Each joint of its link (arm) locates at the root of the link where the parent link connects with.

### 3.2 Kinematics analysis

The kinematics analysis guides actuator selection and geometric design and optimization. Here, since the robot is a 12-DOF, and the identical leg has three actuators at the forearm, the main arm and the shoulder, the leg can have several trajectories. Therefore, starting the kinematics study from a reasonable trajectory is a proper solution. For instance, as the trajectory of Cheetaroid II in Figure 5 illustrates, the lower half of the loop has a straight part of 400mm. This range is where the tiptoe has static friction against the ground and moves the robot forward.

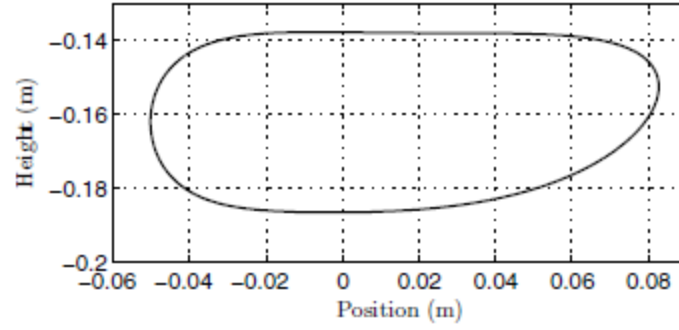


Figure 5 Tiptoe trajectory of Cheetaroid II [2]

For the research, a similar trajectory loop is created in the whole length of 290mm with a straight part of 54.56mm for static friction. Since the leg motion for moving straight only involves joints at the forearm and the main arm, via the motion study, the changes of angular velocities and angular accelerations can be generated at these two joints.

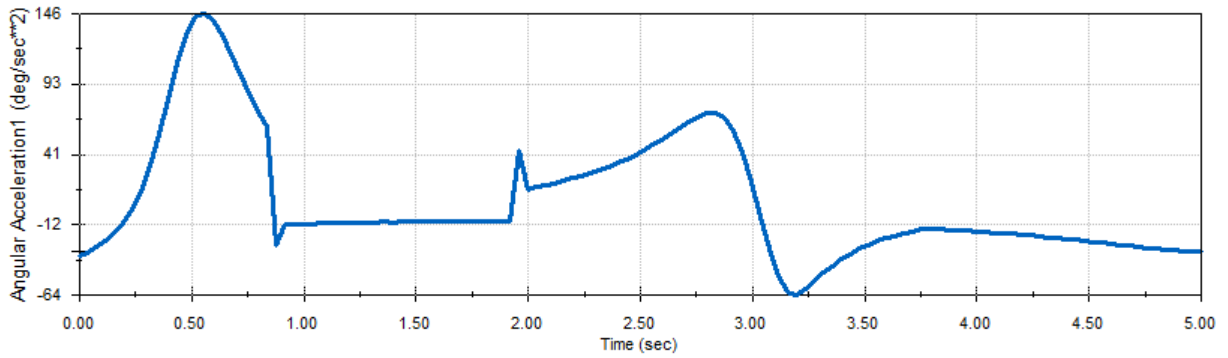


Figure 6 Angular acceleration at forearm joint

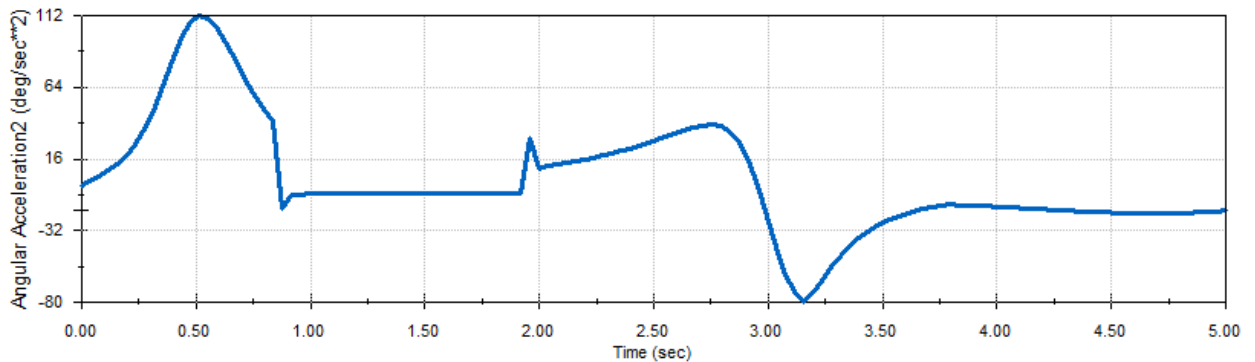


Figure 7 Angular acceleration at main arm joint



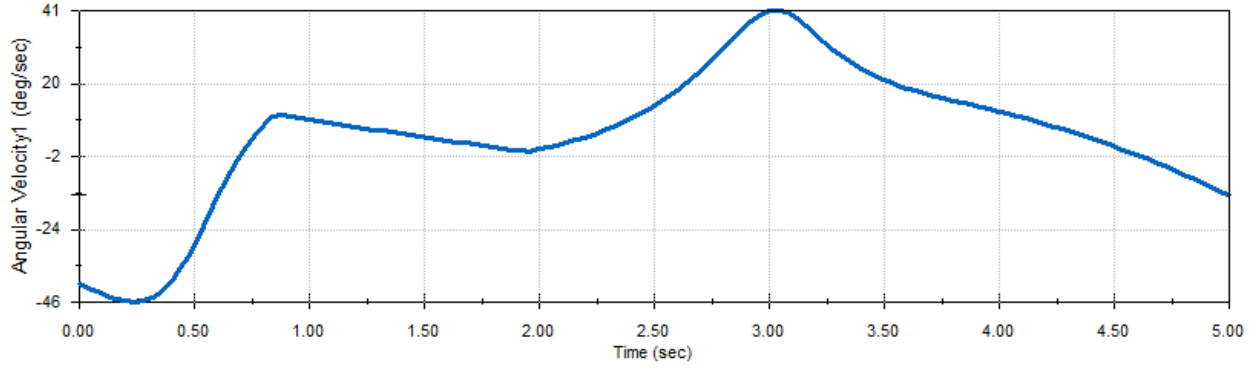


Figure 8 Angular velocity at forearm joint

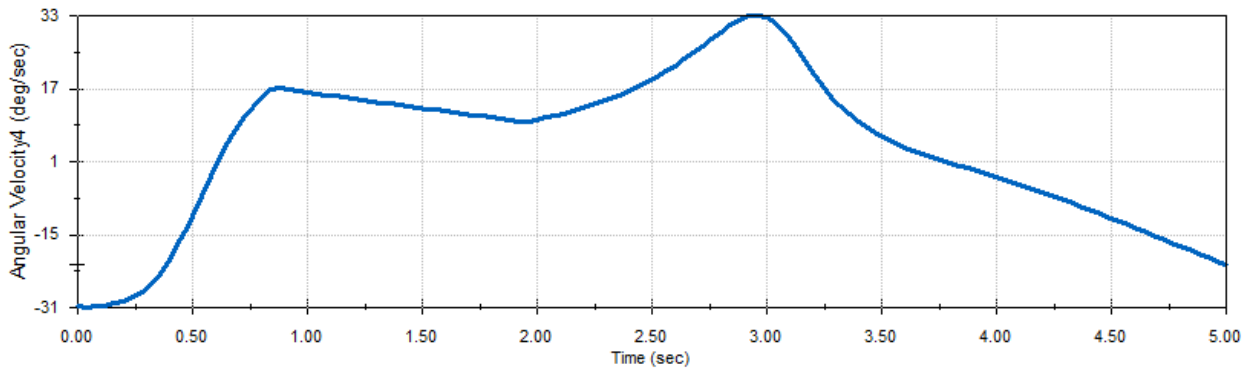


Figure 9 Angular velocity at main arm joint

From the four figures above, we can know the maximum angular acceleration and velocity at the forearm joint is  $146 \text{ deg/sec}^2$  and  $46 \text{ deg/sec}$  respectively, and the maximum angular acceleration and velocity at main arm joint is  $112 \text{ deg/sec}^2$  and  $33 \text{ deg/sec}$  respectively.

With these numbers, the worst cases of load on each part of the identical arm can be estimated. Several assumptions of mass properties need to be setup. Firstly, the weight of the main body with payload is evenly distributed to each leg and is located at the shoulder. Secondly, the center of mass of each part of arm and its actuator is installed at the middle of its length; therefore, the CM (center of mass) of the forearm is at 113.5mm from its joint, the CM of the main arm is at 85mm from its joint. Next, the mass of the forearm and its actuator is 400g and

the mass of the main arm and its actuator is 600g. Eventually, there are two of the four legs touching the ground all the time.

There are several scenarios where the worst case can happen. Due to the tiptoe of one leg not touching the ground all the time, the joints could potentially have the maximum load when the leg touches the ground. When the object is at the point where the distance from the center of mass to the joint is perpendicular to the gravity, the maximum load could potentially occurs as well. Therefore, these scenarios need to be compared. The load on each joint expresses as torque which can be calculated as:

$$J = m \times r^2$$

$$\tau = J \times \alpha \text{ or } \tau = m \times g \times r$$

where  $\tau$  is the torque applied,  $J$  is the moment of inertia of the object,  $m$  is the mass of the object applied on the joint,  $r$  is distance from the center of mass of the object to the joint, and  $\alpha$  is the angular acceleration of the joint.

Known from  $t = 1$  sec to  $t = 2$  sec, the angular accelerations at the forearm joint and the main arm joint is  $12 \text{ deg/sec}^2$  and  $8 \text{ deg/sec}^2$  respectively based on the plots shown before. With the global maximum values of accelerations and others, the generated results can make the comparison.

Table 1 Comparison of the torque load on the joint

Forearm	Torque of the globally maximum angular acceleration	0.7523 N-m
	Torque of the on-ground angular acceleration	0.2254 N-m
	Torque of the self-mass	0.4454 N-m

Main arm	Torque of the globally maximum angular acceleration	0.8092 N-m
	Torque of the on-ground angular acceleration	4.235 N-m
	Torque of the self-mass	1.6128 N-m

From the table of the comparison, the worst case of the forearm is when the torque is 0.7523 N-m and the worst case of the main arm is when the torque is 4.235 N-m. These values become the requirement for the qualified actuators.

### 3.3 Approaches of the concepts of the transformation mechanism / actuators selection

In the concern of the transformation function, placing the transformation mechanism at the leg is more ideal than placing it at the main body. The reason of doing so is that the wheeled structures follow the rules of vehicle dynamics, and planting the mechanism at the legs can share actuators with legged structure. This solution is then planting the mechanism at the body and having an independent driving system which implies unnecessary mass. Therefore, the only reasonable place to plant the transformation mechanism on the leg is the forearm joint for performances and available space.

Given the settled location, there are two approaches of the concepts of the transformation mechanism. Since the motion of the joint features the frequent change of rotation direction and high rotation speed, the two qualified solutions are two-actuator-package and clutch-motor-package.

- Two-actuator-package

The two-actuator-package solution is to use a servo and a motor as actuators. Servo is for the working of the legged structures, but it also functions as the switch for the pre-work by activating the wheeled structure. Figure 10 below explains the working logic of this approach.

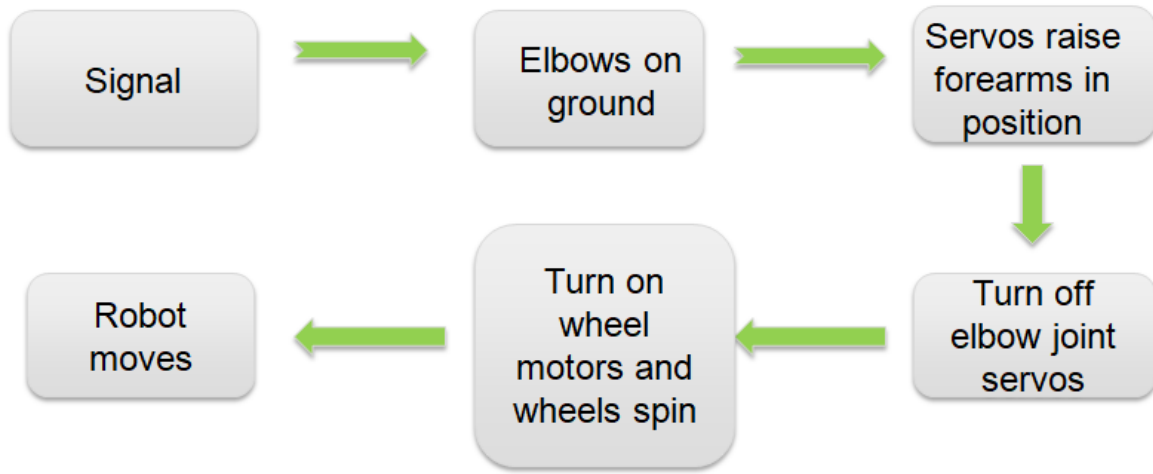


Figure 10 Working logic of two-actuator-package

Based on the constraints of torques and angular velocities calculated above and requirements mentioned in chapter section 2.1, two servos produced by JX Electronic Technology [7] and one motor produced by Pololu Robotics & Electronics [8] are selected. Table 2 shows the parameters of the servos and the motor, and their locations.

Table 2 Parameters of actuators of two-actuator-package

JX CLS-12V7346	Mass	73g
	Operating speed at 14V	0.1sec/60deg (600deg/s)
	Stall torque at 14V	46 kg-cm (4.51 N-m)
JX PDI-HV2060MG	Mass	200g
	Operating speed at 7.4V	0.13sec/60deg (461deg/s)
	Stall torque at 7.4V	62 kg-cm (6.082 N-m)

Polulu 378:1 Metal Gearmotor	Mass	110g
	Free-run-speed at 12V	14 rpm (84deg/s)
	Stall torque at 12V	320 oz-in (2.26 N-m)

Since the torques and the velocities of these actuators are more powerful than the requirements, the approach of the two-actuator-package is valid.

- Clutch-motor-package

The clutch-motor-package solution is to use one motor and one micro electromagnetic tooth clutch. The motor is responsible for both the legged structure and the wheeled structure. The micro electromagnetic tooth clutch purely functions as the transformation mechanism.

Figure 11 below explains the working logic of this approach.

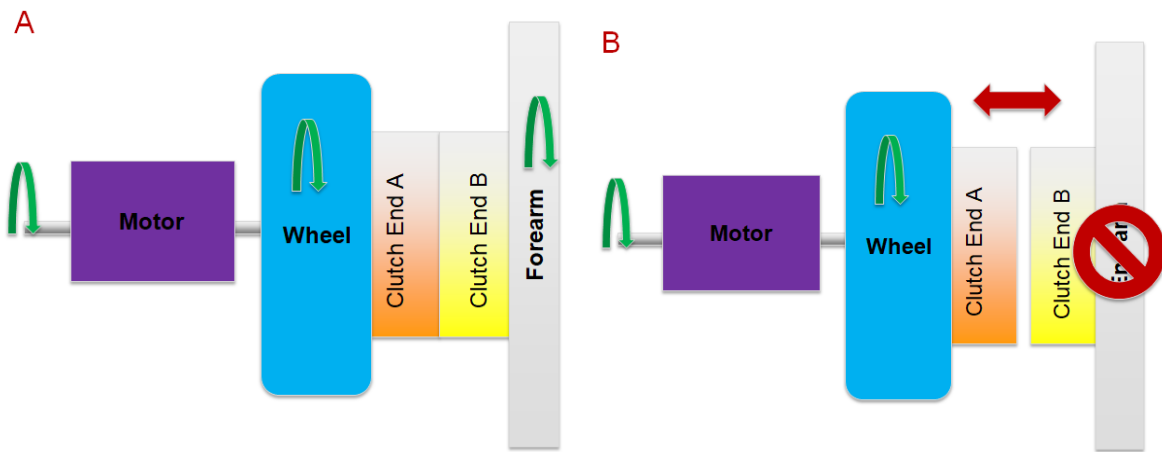


Figure 11 A: legged structure mode; B: wheeled structure mode

At the mode of the legged structure, the wheel spins with the forearm as the tooth clutch ends attaches each other. After transformation, the clutch detaches, and the motor only drive the wheel at this moment. In summary, this approach has the wheel spinning all the time, and requires an additional mechanism to lock the free-moving forearm after transformation.

However, these defects are not worse than the difficulty on the clutch selection.

Since the motion of the joint features the frequent change of rotation direction and high rotation speed, only the electromagnetic clutch is qualified. Due to the limit of the robot mass, the mass of the clutch needs to be light. Through the Internet, the micro electromagnetic tooth clutches produced by Miki Pulley [10] and ICP [11] are the options that are closest to the requirements but still unqualified.

Table 3 Parameters of micro electromagnetic tooth clutches

	Miki Pulley 546-12-34	ICP METC 0.5
Torque	17.5 N-m	6.3 N-m
Exciting voltage	24V	24V
Diameter	57mm	42mm
Mass	500g	330g

These two clutches listed in Table 3 are the qualified options. Although the torques they can offer are strong enough for the leg motion and the wheel motion, they are oversized, which limits the forearm joint's motion space. The mass of each is also too heavy. With the mass of the motor of 110g and the mass of the main arm servo of 200g, the sum of the mass of actuators for one identical leg reaches 640g at least. This leaves only 360g of the mass for the rest part of the leg, which can compromise the strength of the solid structure. Given that, the approach of the clutch-motor-package is invalid.

### 3.4 D printing study

3D printing is an additive layer manufacturing method that uses materials of plastics, metals and resins to create 3-dimensional objects [12]. 3D printing features the low time

consumption, low cost, and accuracy. The processes of metal-printing and plastic-printing are very different. In this research, the main materials are PLA and ABS.

The 3D printer's key parts are the extrusion nozzle that deposits the material to form the layer in as programmed, and it raises its height for the work of another layer. The way of the material deposit leads to an issue on the part strength.

When the load is applied on the direction perpendicular to the plane of the material layers, the part is holding bending stress from the load. The part is strong at this direction. However, when the load is applied along the material layers, the part is holding shear stress from the load. Since the mechanical weakness of the parts is at the connections between each pair of layers, a shear stress smaller than the bending stress may tear the part apart [12].

Another feature of 3D printing is that the printed part is not solid inside. The printer deposits materials to form tiny lattices during printing. Those lattices function as inner structures of the printed part. The outer layers of the printed part have more concentrated material deposit than the inner. Therefore, for 3D printed parts, a flat solid designed block is weaker than the same sized board with slots as rough outer surfaces.

## Chapter 4: Design of the transformable quadruped robot

This chapter introduces the key parts of one identical leg assembly each by each. Figure 12 below displays the complete assembly of the leg.

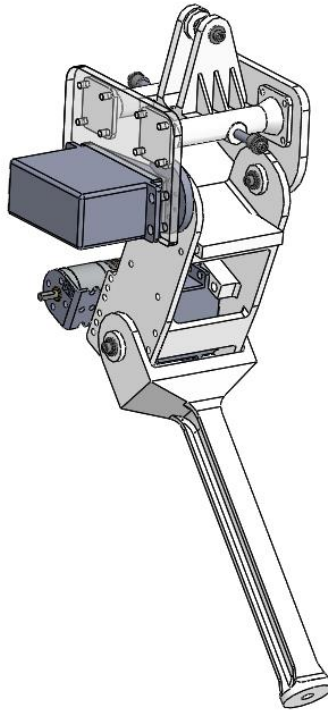


Figure 12 Complete assembly of the leg

### 4.1 Design of the forearm

Since the forearm holds bending stress, the major part of the forearm is designed to be an I-beam for quality performance on bending stress and less mass at the same time. The whole forearm is printed up from the servo arm bracket side. On the near end of the forearm (revolute joint location), a flange is designed for sleeve bearing fitness because the length of the bearing is longer than the thickness of the end of 4mm. On the opposite is the servo arm bracket. In the



reality, the bracket uses 8 M2 bolts rather than 12 due to interferences. Fillets at the connections of ends are to transmit load to the whole forearm structure.

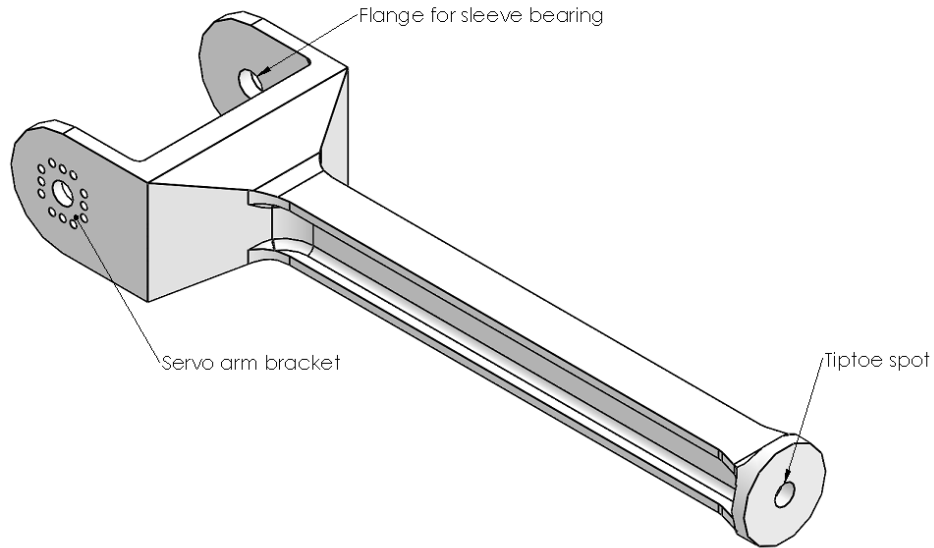


Figure 13 Prototype of the forearm

#### 4.2 Design of the main arm

The main arm is an assembly comprising two 3D printed boards in the thickness of 4mm and sleeve bearing-shaft subassembly. The main arm assembly includes the forearm servo and the wheel motor. To reduce the moment caused by the servo and the motor, the joint-to-joint distance of the main arm is reduced to 100mm.

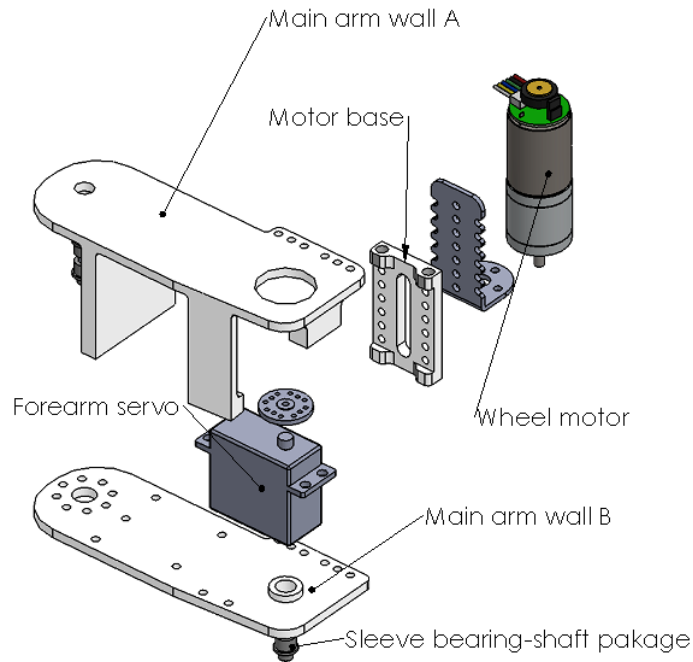


Figure 14 Exploded view of main arm assembly

The design stage of this part experiences several modifications for assembly and performance. The first version of the main arm has different forearm servo seat and close-located cross-supports. On the main arm of the first version, the forearm servo seat was bolted on one of the cross-support. One issue of this design is the servo seat cannot hold the servo tight because of the reaction torque the working forearm servo generates.

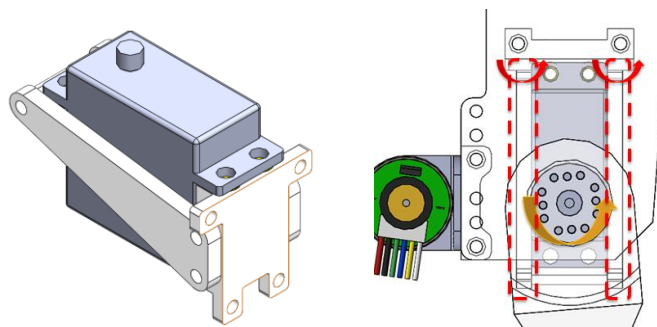


Figure 15 Left: former forearm servo assembly; right: weak seat causes reaction torque

Another issue is that one of the cross-supports blocks the path to engage the tools. Since the main arm packs the forearm servo colinearly with the forearm joint shaft, the servo installment requires sticking the wrench into the main arm package.

Based on the defects above, the final version of the main arm has a redesigned forearm servo seat which integrates the side part of the main arm assembly. The modification change the servo installment to being bolted with four M4 bolts, which provides strong strength to balance the reaction torques. Additionally, the blocking cross-support is moved to other location. This solves the assembly issue without damaging the structure strength.

#### 4.3 Design of the shoulder

The shoulder is an assembly comprising one acrylic board for the main arm servo seat and the connection part functioning as a rocker as shown in Figure 16 below.

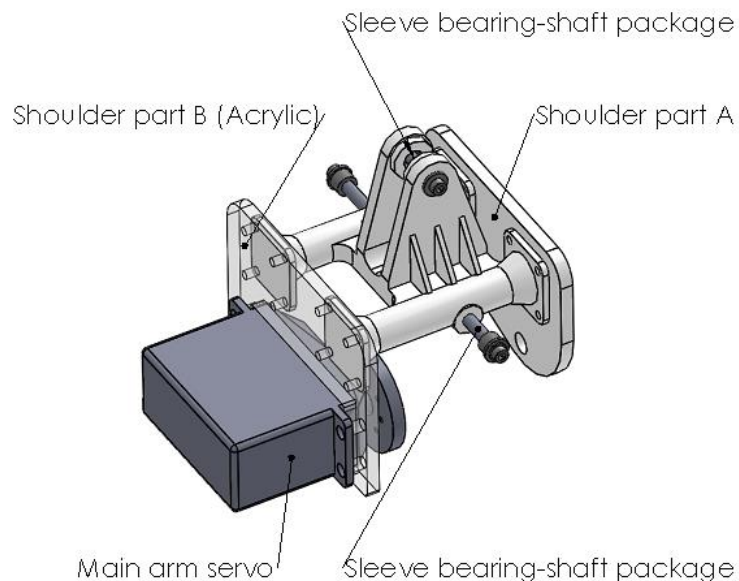


Figure 16 Shoulder assembly

The design stage of the shoulder also experiences several modifications. The first version of the shoulder assembly comprised three parts: two boards of the main arm servo seat and the

sleeve bearing seat and the connection part. Since the shoulder joint is close to the board of sleeve bearing seat, the space for the bolts and the nuts is squeezed so that the tool cannot engage. Accordingly, the board and the connection part are combined to be one, and all the bolt holes are removed. Another modification is at the shoulder joint. At the joint of the first version, the shaft touches the shaft hole surface. Since the 3D printed part surface is not smooth, touching the surface generated extra friction and damages the part. Therefore, a set of sleeve bearings is placed at the shoulder joint to isolate the shaft and the 3D printed part.

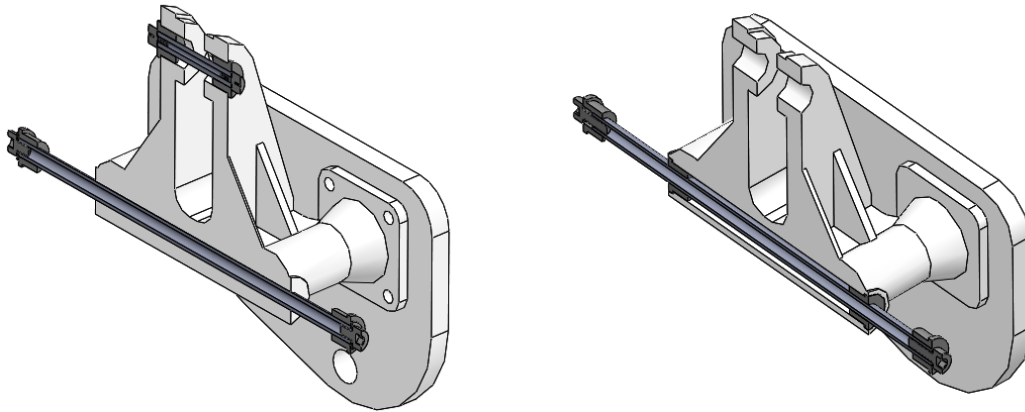


Figure 17 Left: old design without isolation; right: current design with isolation

#### 4.4 Design of the transformation process

As the elbow servo manages the transformation, there is no need to have an independent mechanism. The process of the transformation turns is simple and fast. Figure 18 below shows the logic of the process on the mechanical aspect.

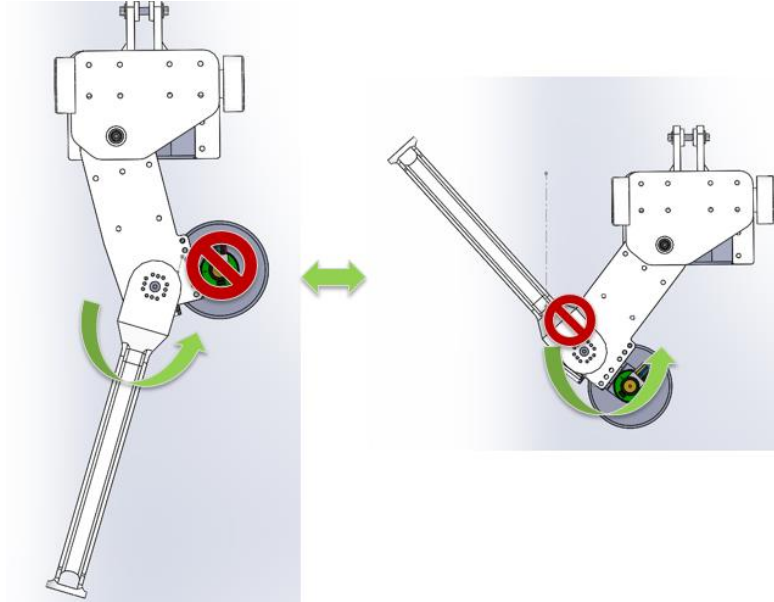
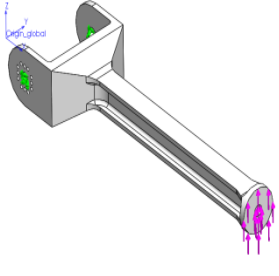
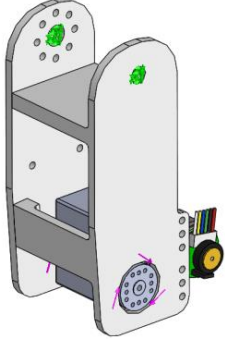
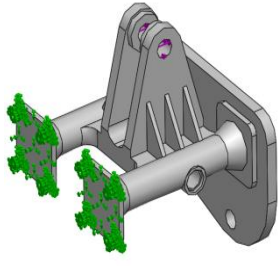

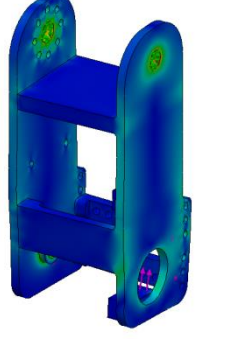
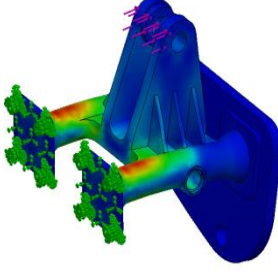


Figure 18 Transformation process

#### 4.5 Simulation of designed parts and assemblies

The simulation is to simulate if the parts would fail under the worst scenario. For each part and assembly, the worst scenario could be different. For the forearm, the bending stress and the compression often exert on it. Therefore, those two are worst cases. For the main arm assembly, its worst case is it faces the huge torque generate by the forearm servo. For the shoulder assembly, the bending stress along the width of the robot is the worst scenario. Below is the table of the parts' and assemblies' stress performances in their worst scenarios using simulation functions in Solidworks.

Table 4 Parts' and assemblies' stress simulation

	Forearm	Main Arm	Shoulder
Applied Force at the Worst Case			
Stress Performance			
Maximum Von Mises Stress	$2.07 \times 10^7 \text{ N/m}^2$	$2.49 \times 10^7 \text{ N/m}^2$	$2.44 \times 10^6 \text{ N/m}^2$

The results returned from the simulation show that all the parts and assemblies survive the worst scenarios. The Von Mises Stress closet to the PLA yield strength ( $3.0 \times 10^7 \text{ N/m}^2$ ) is  $2.49 \times 10^7 \text{ N/m}^2$ . The hand-calculation is needed to double check the validity of the simulation.

The hand-calculation of the forearm is stated as a sample. The shape of the forearm is I-beam alike. Known the length of the I-beam is 151mm and the dimensions of the cross section is, the moment of inertia can be calculated in ref.[13] as:

$$I = \frac{1}{12} b_1 h_1^3 + \left( \frac{1}{12} b_2 h_2^3 + A_2 d_1^2 \right) + \left( \frac{1}{12} b_3 h_3^3 + A_3 d_2^2 \right)$$

where the cross section of the I-beam is split to three parts for convenience;  $b$  is the width of each part;  $h$  is the height of each part; and  $A$  is the area of the part off the neutral axis;  $d$  is the

distance from the part to the neutral axis as the Figure 19 shown below. All numbers are in millimeters.

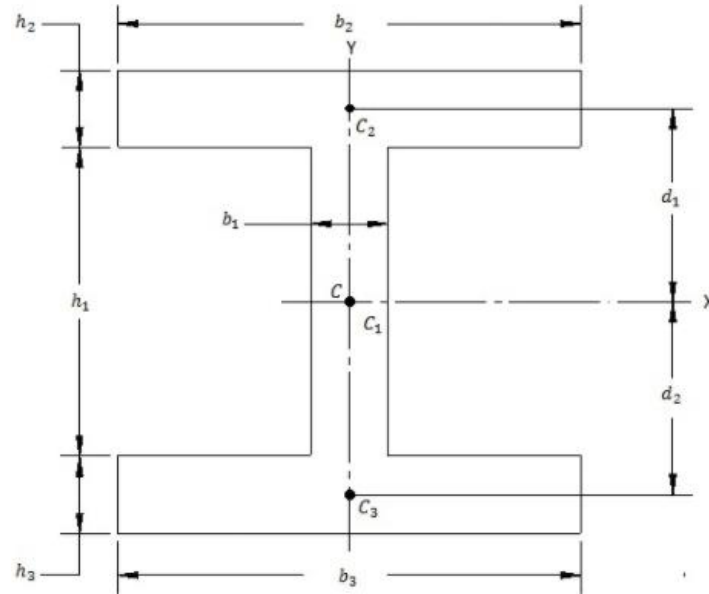


Figure 19 The schematics of the forearm's cross-section [14]

After knowing the moment of inertia of the cross-section, the bending stress at the joint-side of the I-beam can be calculated in ref. [15] via:

$$S = \frac{wl}{I/y}$$

where  $S$  is the maximum bending stress happening at the root;  $w$  is the equivalent force applied on the end of the I-beam;  $l$  is the length of the beam;  $I$  is the moment of inertia; and  $y$  is the distance from the neutral axis to the edge.

Eventually, the hand-calculated value of the maximum bending stress of the forearm is  $7.99 \times 10^6 \text{ N/m}^2$ , which is almost the same as the simulated value of  $8.64 \times 10^6 \text{ N/m}^2$  at the same place. Therefore, the simulation is valid.

#### 4.6 Trajectory generation

Nevertheless, the corresponding angular displacements of both servos are calculated from the inverse kinematics, this calculation is executed by Solidworks Motion Analysis. To assign the robot itself the capability of generating the angular displacement, the inverse kinematics function should be planted into the robot's controller.

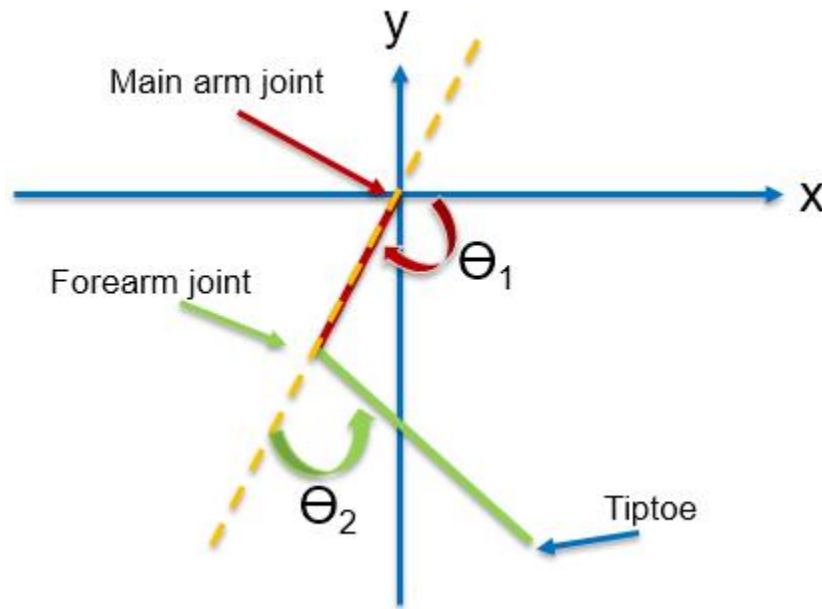


Figure 20 Coordinate system setup

The inverse kinematics function refers to the coordinate system shown in Figure 20 above. The angular displacement of the main arm refers to the x-axis, and the angular displacement of the forearm refers to the main arm. Accordingly, the angular displacement and the tiptoe location (x and y) have the relationship as:

$$x = L_1 \cos \theta_1 + L_2 \cos(\theta_1 + \theta_2)$$

$$y = L_1 \sin \theta_1 + L_2 \sin(\theta_1 + \theta_2)$$



where  $L_1$  is the length of the main arm, and  $L_2$  is the length of the forearm. With the two equations, the value of  $\theta_1$  can be calculated at the first:

$$\cos\theta_2 = \frac{x^2 + y^2 - L_1^2 - L_2^2}{2L_1L_2}$$

$$\theta_2 = \arccos\theta_2$$

known the value of  $\theta_2$ , the value of  $\theta_1$  can be calculated by substituting  $\theta_2$  into either of equations below:

$$x = (L_1 + L_2\cos\theta_2)\cos\theta_1 + (-L_2\sin\theta_2)\sin\theta_1$$

$$y = (L_1 + L_2\cos\theta_2)\sin\theta_1 + (L_2\sin\theta_2)\cos\theta_1$$

Thus, one unique relation between  $\sin\theta_1$  and  $\cos\theta_1$  is learned. With the basic relation between  $\sin\theta_1$  and  $\cos\theta_1$ :

$$\cos^2\theta_1 + \sin^2\theta_1 = 1$$

The value of  $\theta_1$  can be calculated via:

$$\theta_1 = \arccos\theta_1 \text{ or } \theta_1 = \arcsin\theta_1$$

With the inverse kinematics function planted in the controller, the robot can generate trajectories itself. The x's and y's coordinates can be functions in term of time, then the controller can control the speed. Following figures show the result of the inverse kinematics function with the input of 5 sets of tiptoe coordinates of key points as the samples.

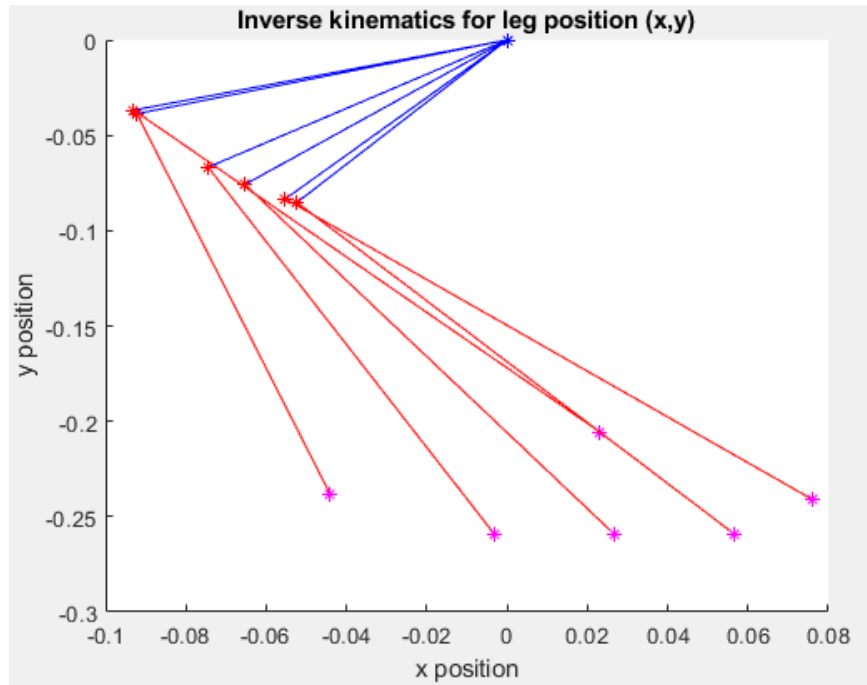


Figure 21 Inverse kinematics for leg position

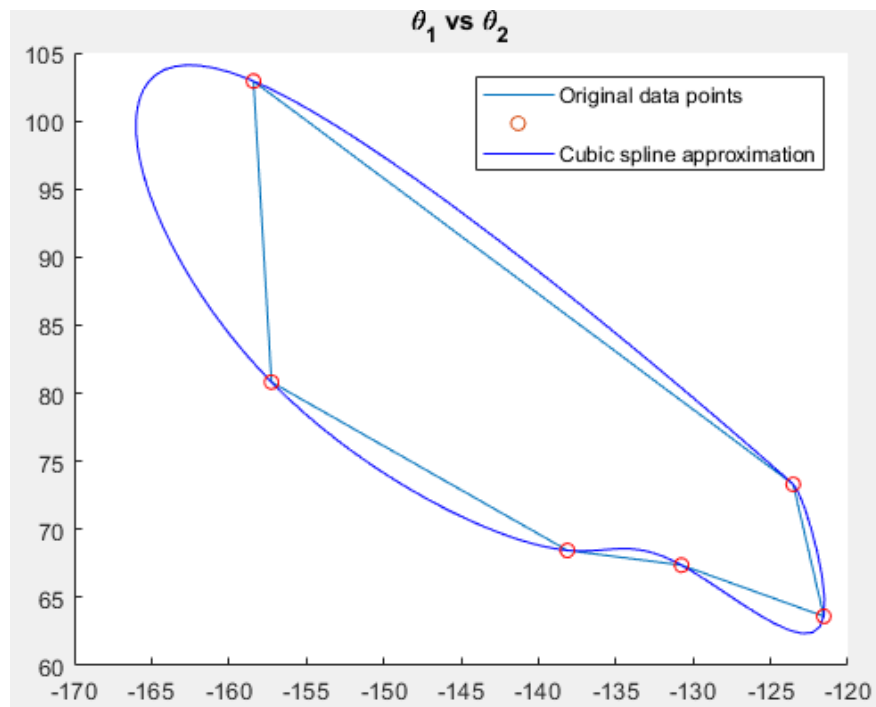


Figure 22 Sets of  $\theta_1$  and  $\theta_2$  generated by the function

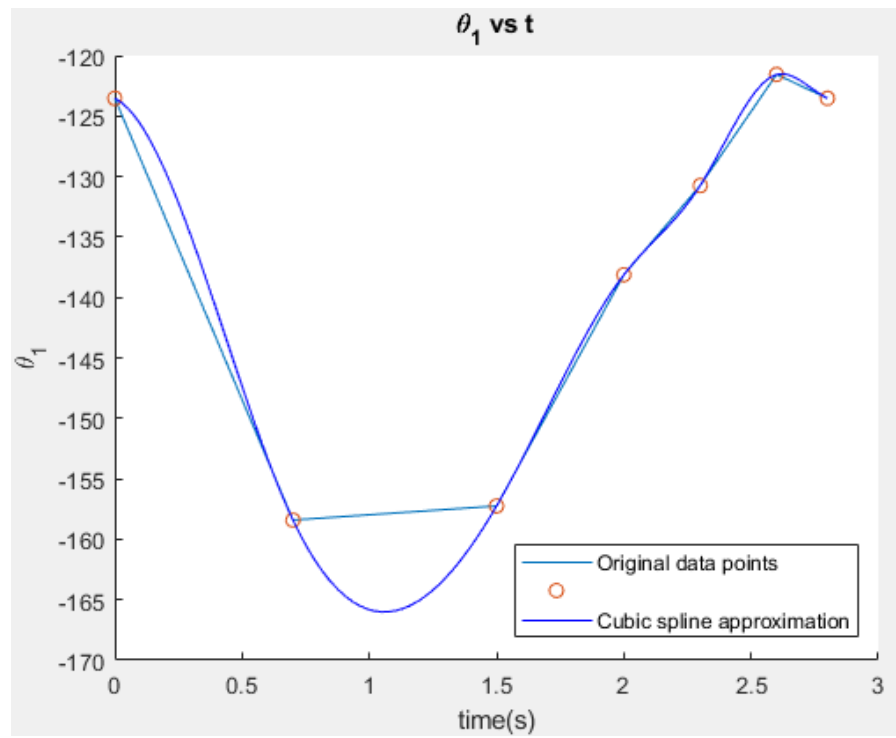


Figure 23 Angular displacement  $\theta_1$  vs. time

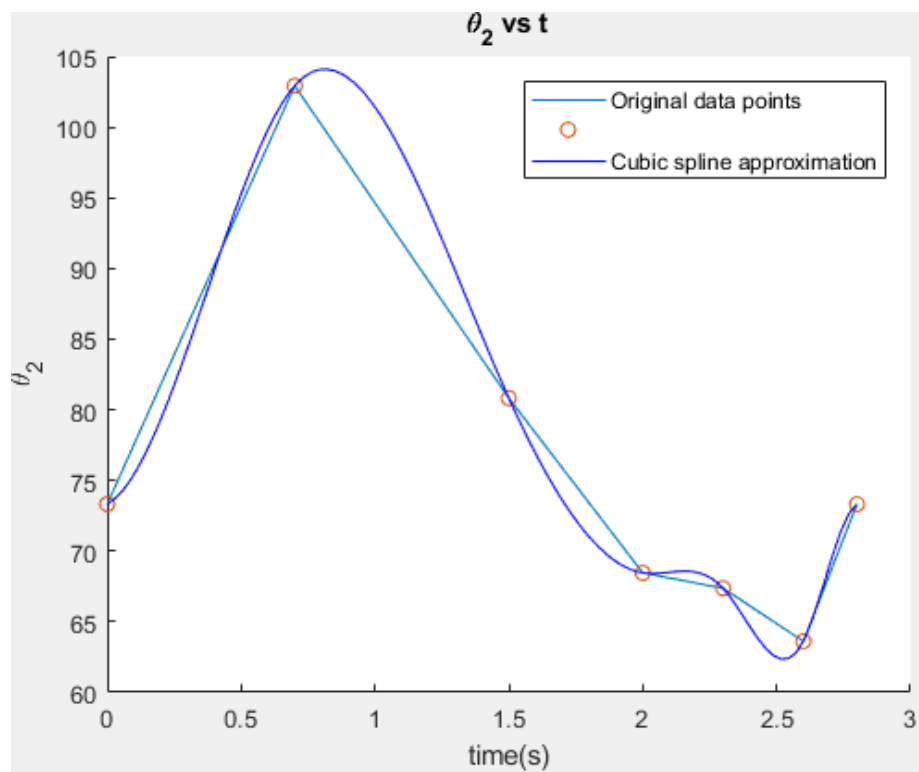


Figure 24 Angular displacement  $\theta_2$  vs. time

## Chapter 5: Testing procedures and results

Given the one of the four legs is created and assembled, this chapter is about the testing goal, the setup of the tests, detailed testing procedure, results of different tests and discussion.

### 5.1 Goal of testing

The purpose of the testing is to verify if the servos can work within the designed structure: whether they can reach the target angles in time as programmed or not. It is also to learn in what conditions the servos can have quality work. The features and the control performance can show via the comparison between the designed tiptoe trajectory and the actual projected trajectory.

### 5.2 Testing setup

Firstly, apply the whole leg assembly on a stationary clamp. Place the camera a certain distance from the leg so that the camera can record the complete motion of the leg. Connect the servos to the control board, Arduino, and power, then connect both the board and the Arduino to the computer for importing code and observing feedbacks.

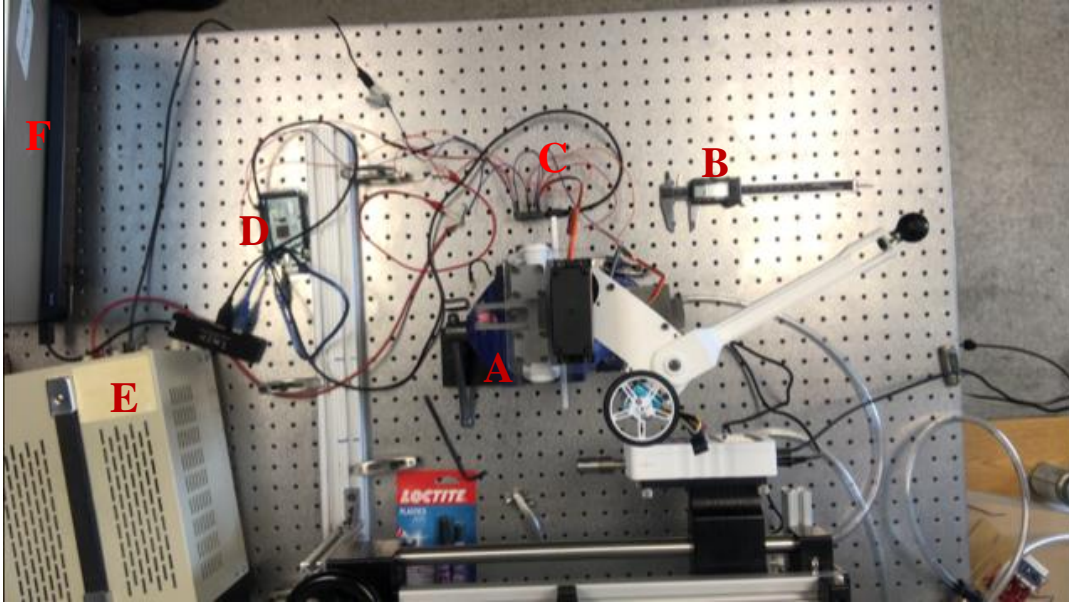


Figure 25 A: clamp; B: caliper for calibration; C: control board; D: Arduino; E: power; F: computer

Secondly, import the angular displacements from the trajectory generation to the code of the leg motion. The plots of angular displacements vs. time steps are shown in Figure 26 and 27 below.

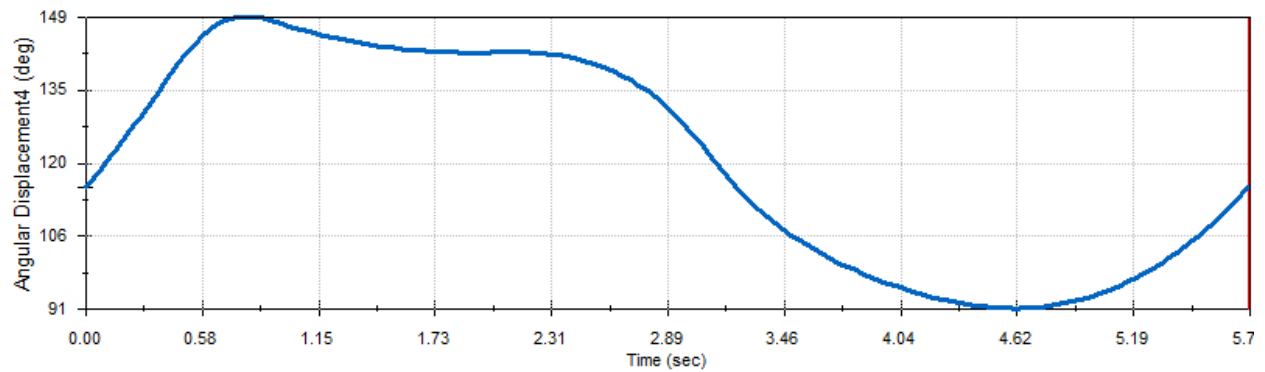


Figure 26 Angular displacement of the forearm servo

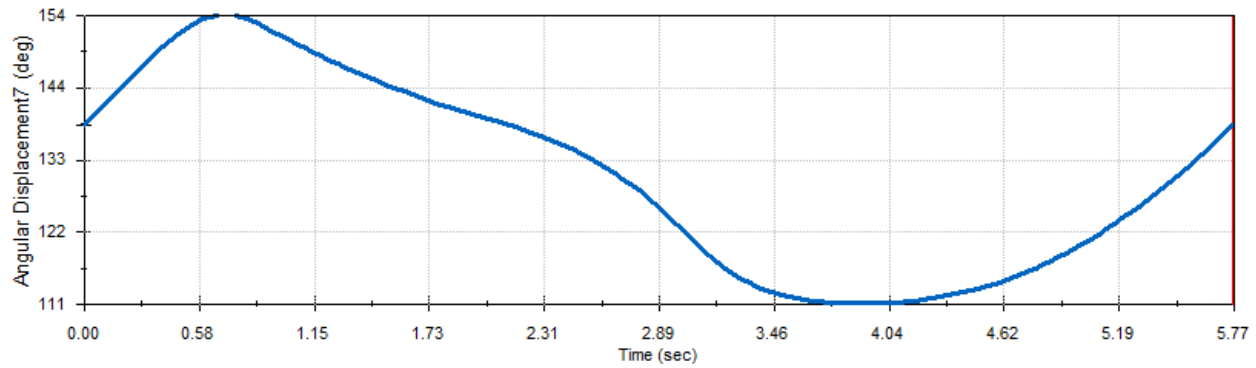


Figure 27 Angular displacement of the main arm servo

With these values, the next step is to zero the corresponding servos the same as the initial status in the motion study.

Finally, power on the circuit and translate those corresponding angular displacement values to the numbers the servos can read. Use the camera to record the whole leg motion for several cycles. Then import the video file to Tracker (motion analysis software). Tracker calculates the tracing point location at each moment, and scales the data via the caliper included in the video. Figure 28 shows the operating screen during the analysis.

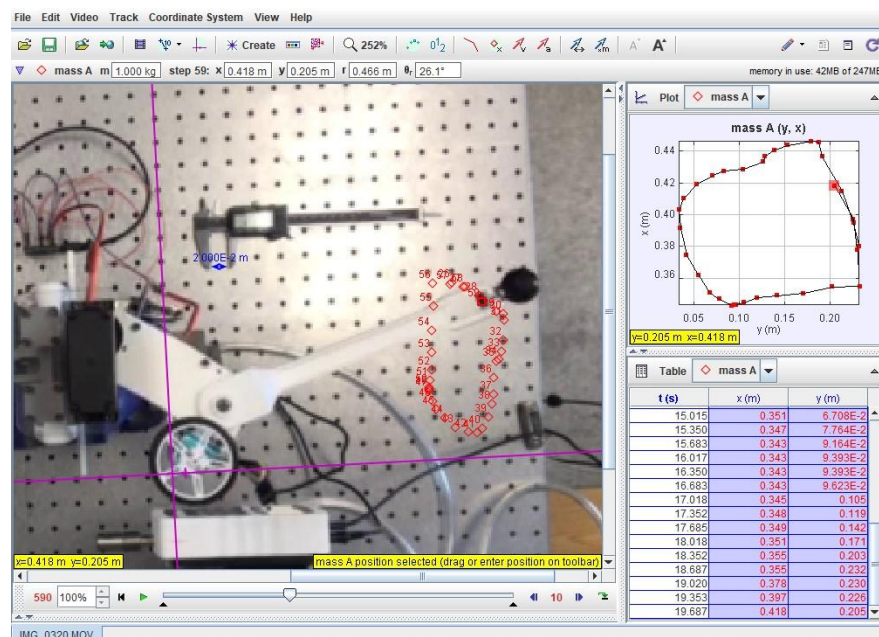


Figure 28 Operating screen of Tracker

### 5.3 The testing procedure

1. Lock the forearm servo, run the main arm servo only, then record the motion via the camera. The reason is that the whole leg motion is the two servos cooperation; therefore testing single servo's working performance can help locate the potential hardware issue in the future. Since the revolute joint of the main arm servo is fixed, it is an ideal option for this step.
2. Import the original angular displacement database to the corresponding servos, then run the main arm servo and the forearm servo both without delay. Use the camera records the motion.
3. Evenly divide the whole trajectory to several key points. Run the main arm servo and the forearm servo both, import the filtered angular displacement database to the corresponding servos without delay, then use the camera record the motion.
4. Run the main arm servo and the forearm servo both, import the filtered angular displacement database to the corresponding servos with delay, change the frequency (the number of angular displacement values sent to the servos per second), then use the camera record the motion.
5. Compare the designed trajectory from the motion study with the one from the former three steps respectively, observe the loop paths, then make conclusions.

### 5.4 Testing results

The testing results of the first procedure reflect that the servos can roughly follow the trajectory as programmed. During the process of following the programmed trajectory, the

servos turn slowly with abnormal shakes at the same time. In the second procedure, the issue does not change via reducing the number of the key points sent to the servos per second.

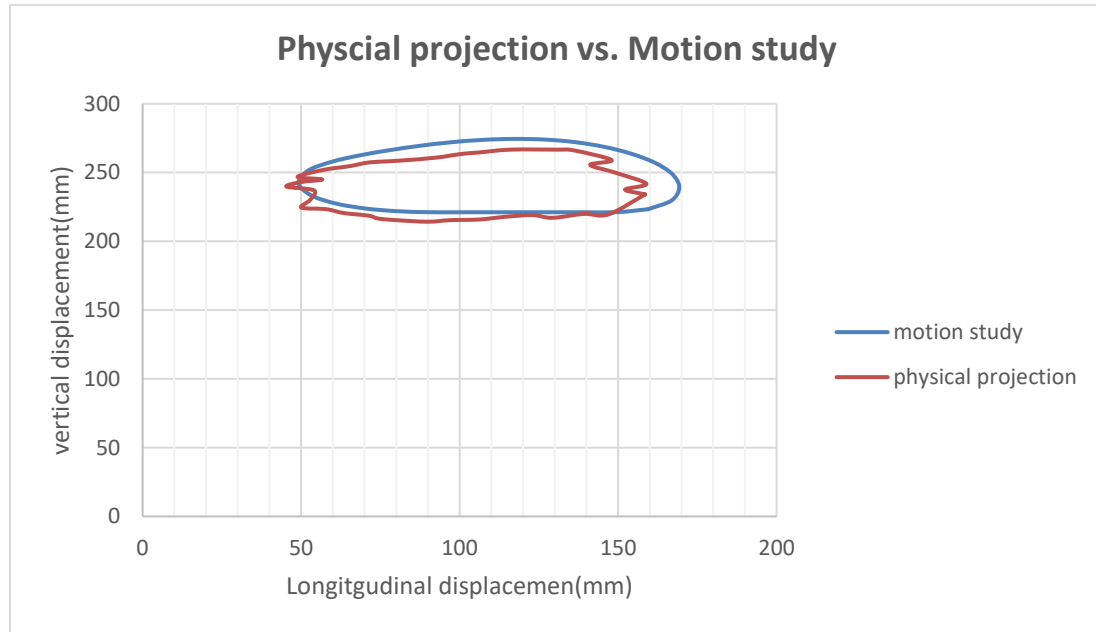


Figure 29 Comparison between actual motion loop and the designed trajectory at step 1

The team infers that the root of the issue is at the key points itself. After speculating the data sent to the servos, the team found that the key points resolution is smaller than the accuracy of the servos. The servos realize the differences of the target angles/signals but cannot properly execute the orders. Hence, the servos act like jam.

Given the feedback from the first procedure. The third procedure reduces the number of the key points via evenly dividing the whole trajectory to 21 points. In the result, the shakes and jam of the servos are barely seen.



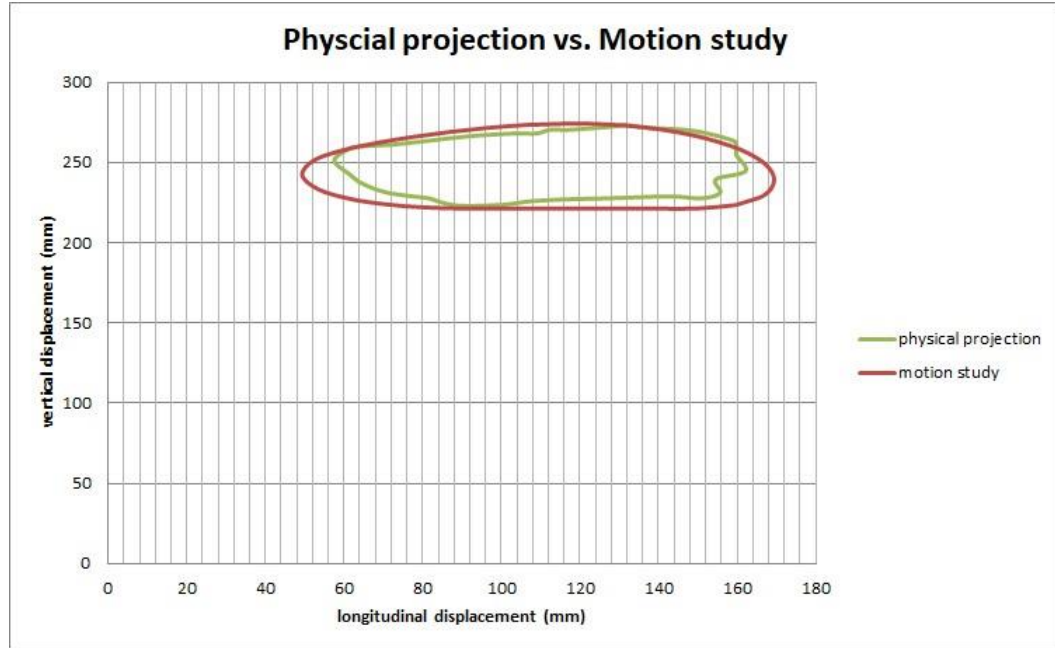


Figure 30 Comparison between actual motion loop and the designed trajectory at step 3

Therefore, as Figure 30 shows, the actual trajectory of the leg motion is smoother than before. The ground-contact section is very similar to the one from the motion study trajectory.

In the 4<sup>th</sup> step of the testing, the filtered 21 segment critical points are still the database, and the controller introduces the frequencies (the number of signals sent to the servo per second) of 40 Hz and 20 Hz respectively to exam the quality of leg motion in different speed.

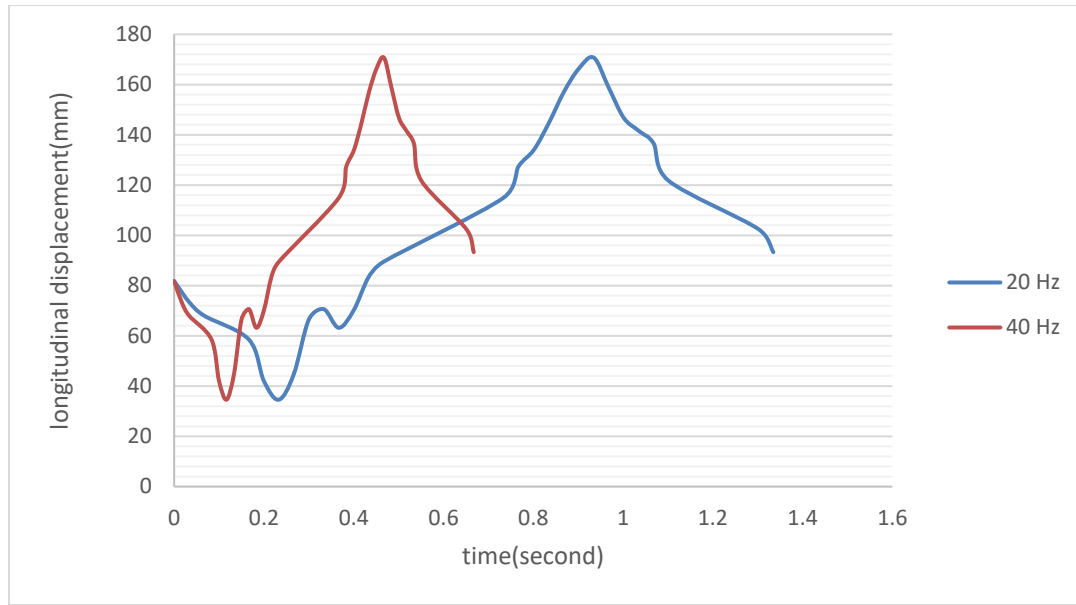


Figure 31 Comparison between time consumed for one cycle in 20 Hz and 40 Hz

Based on the result, the servos do not experience a significant compromise on its performance of completing the leg motion in different frequencies.

### 5.5 Discussion of the leg motion testing

From the results from the testing, we can make conclusions that can guide the future leg motion setup and tuning:

- The angular displacements exceed the servo motion accuracy in the allowable tolerance can cause unsmooth motion and motion jam.
- Reducing the number of key points can remove the motion jam and significantly reduce the roughness of the actual trajectory.
- The servos do not experience a significant compromise on its performance of completing the leg motion in different frequencies.

In conclusion, although there are errors between the actual trajectory and the motion study one, the actual one is the same as the designed. It is inferred that the errors are caused by the camera. Since the analysis uses videos as samples, the quality of the videos is essential. In these tests, the camera can only film at 60fps [16] as the maximum. Therefore, some moments of the tiptoe location are missed. The video resolution is also not so high that the scale of the actual path might have some tiny difference against the designed one. Using a better camera and recording as more cycles may shrink the size of the errors.

## Chapter 6: Conclusions and Future Work

### 6.1 Contributions

This thesis explores the possibility of the commercial actuator application on robotic mechanisms. Many previous robots in the similar scale were created to use customized actuators. The advantage of using customized actuators is high performance and more compact design. However, customized actuators also are costly. They may not last for long since some changes on them could abuse parts on the actuators, then damage the whole things far by its designed lifespan. For this scale of legged robots ( $0.166 \text{ m}^3$ ), using commercial actuators can properly complete the motion job. Although the quality of motion on accuracy is not fine as customized actuators, the completed motion is good enough for this scale of robots. And the engineered pattern of using the commercial actuators has the potential to easily apply on other similar sized but different structured robots, which is tough for customized actuators.

The thesis also explores the transformation mechanism design that can swap a robot from wheeled structure to legged structure or vice versa. Wheeled structure and legged structure have different theories of moving. Having both structures and ability of transformation without damaging the durability of the structural strength and the pay load of the robot becomes an issue. This thesis offers a solution: two independent structures; and using legged structure actuator is control the transformation. This solution eliminates the worries of extra weight of transformation mechanism and damage of the structural strength.

## 6.2 Future work

### 6.2.1 Mechanical design

- The shaft is sealed on both ends by compatible screws. Since the motion of parts can create torsion on the shaft itself, either of the two screws on ends can be loosen by the torsion. Once the shaft is unsealed from both ends, the shaft falls out the joint. During the testing, the team find some loosen screws after several cycles of run. To solve the issue, replacing the screws by retaining rings is a good way since the force by the torsion is not along the force direction to expand a retaining ring. Therefore, the shaft can sit tight in the joint.
- Adding a passive suspension system to each leg. The leg has no suspension; therefore, the impact from the hard contact transmits to the whole robot. Considering the 3D printed part is weak along the impact direction, a suspension system is a high demand for future work. One valuable inspiration is from MIT's Cheetah [17] as shown in Figure 32.

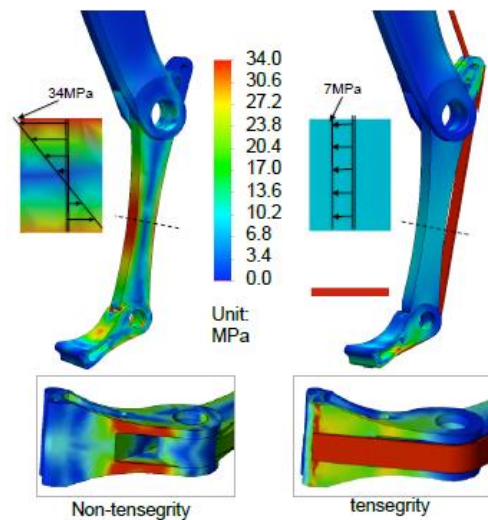


Figure 32 FEA analysis of locked-joint(L) and tensegrity leg(R) under 1000 N vertical load [17]

The suspension part—the fabric band on the forearm—evens the stress distribution on the forearm, and the stress on the joint reduces which is good for actuator at the place.

Designing a suspension like this can reduce the risk of structural failure.

- Complete the build of the whole robot with those changes mention previously. The finished robot at least should be able to be controlled from the computer end and be powered using a power cable.

### 6.2.2 Testing

- Build function model for trajectory generation so that the repeating work on motion analysis in Solidworks can be less, and the controller itself can generate required trajectory without connecting to the computer.
- Start researching the walking motion of the whole robot. This will involve the servo tuning and motion study trajectory refining.
- Start researching the wheeled motion of the whole robot. Although the robot still needs to follow the theory of vehicle dynamics. Its motion of cornering refers a more complex control since its wheels do not steer. The robot will lean to the cornering center and depend on the inner and outer steering radius difference to corner.

### 6.3 Summary

This research is to design and prototype a transformable quadruped robot with its transformation mechanism, so it can transform between the quadruped type and the wheeled type freely depending on the terrain conditions. One identical leg of the robot has been designed, built, and tested. The validity of the prototype leg and the one of the commercial actuator application have been tested. Due to the time limit, the construction of the whole

robot and the testing of the complete robot movement in the two structures are included in the future work.

## Reference

1. Dai, J. S., and Jones, J. R. (1999). Mobility in Metamorphic Mechanisms of Foldable/Erectable Kinds. *Journal of Mechanical Design*, 121(3), 375-382. doi:10.1115/1.2829470
2. Byeonghun, N., and Kyoungchul, K. (2016). Design of a One Degree-of-Freedom Quadruped Robot Based on a Mechanical Link System: Cheetaroid-II. *IFAC-PapersOnLine* 49-21 (2016) 409–415
3. Biorobotics, Laboratory. (2013). Hardware Development on Quadruped Robots. Retrieved from <https://biorob.epfl.ch/op/edit/page-65008.html>
4. Anonymous. (2014). A Simple Quadruped Robot. Coretech Robotics. Retrieved from <http://coretechrobotics.blogspot.com/2014/10/a-simple-quadruped-robot.html>
5. BDI Spot Mini. (2008). Boston Dynamics. Retrieve from <http://bostondynamics.com>
6. Inho, K., Wonseok, J., and Hyunseok, Y. (2017). Design of a Transformable Mobile Robot for Enhancing Mobility. *International Journal of Advanced Robotic Systems* January-February 2017: 1–14
7. Jixian Servos. Retrieved from <http://www.jx-servo.com/english/>
8. Pololu 378:1 Metal Gearmotor. Pololu Robotics and Electronics. Retrieved from <https://www.pololu.com/category/115/25d-mm-metal-gearmotors>
9. Douglass, J, G., (1997) Efficacy of Methods for Estimating In-Service Motor Efficiency. Washington State University Cooperative Extension Energy Program report prepared for the Pacific Gas and Electric Company and the Bonneville Power Administration
10. Miki Pulley 546-12-34. Electromagnetic Tooth Clutches. Retrieved from <https://www.mikipulley-us.com/miki-pulley-us>
11. ICP METC 0.5. Mini Electromagnetic Tooth Clutch. Retrieved from <https://www.industrialclutch.com>



12. Jason, C., Sean, R., David, D., Rishi, G., Luke, D., Josh, A., Andie, Y., Alex, J., Douglas, S., Calvin, K., and Peter, I. Experimental Characterization of the Mechanical Properties of 3D-Printed ABS and Polycarbonate Parts. Mechanical and Aerospace Engineering Department, 571 Gale Lemerand Dr., MAE-C 134, University of Florida, Gainesville, FL 32611., Bartram Trail High School, Saint Johns, FL, 32259., College of Engineering, University of California at Berkeley, Berkeley, CA 94720
13. Jack, A, C., Henry, B., and George, S. (2010). Mechanical Design of Machine Elements and Machines. ISBN 978-0-470-41303-6
14. Anonymous. Strength of Materials: Area Moment of Inertia. Retrieved from [https://sbainvent.com/strength\\_of\\_materials/area-moment-of-inertia.php](https://sbainvent.com/strength_of_materials/area-moment-of-inertia.php)
15. Dupaix, R, R. (2016). Becoming a Finite Element Analyst: A Design-Model-Verify-Approach.
16. iPhone 7 specifications. Retrieved from: <https://www.apple.com/lae/iphone-7/specs/>
17. Sangbae K., and Patrick, M, Wensing. (2014). Design of Dynamic Legged Robots. Foundations and Trends in Robotics. Vol. 5, No. 2 (2014) 117–190. DOI: 10.1561/23000000044